JOURNAL OF APPLIED ENGINEERING SCIENCES
ISSN: 2247-3769 / e-ISSN: 2284-7197

sciendo

VOL. 15(28), ISSUE 2/2025
ART.NO. 452 pp. 183-194

PERFORMANCE AND DURABILITY OF LATERITE SOIL STABILIZED WITH GEOPOLYMER BINDER MADE FROM LOCAL BIO-SOURCED MATERIALS FOR ROAD CONSTRUCTION

M. F. Ahlinhan [a*], B. D. Djenou [a], J. A. Yamonche [b], L. Tokpanou [a]

[a] Research Unit in Geotechnics, Laboratory of Study and Test in Civil Engineering (L2EGC), National High School of Public Works (ENSTP), E-mails: *ahlinhan@yahoo.fr, djenoudorothee@gmail.com, loukmantokpanou@gmail.com
[b] Laboratory of Processes, Innovations and Technologies (LaPIT), National University of Sciences, Technologies, Engineering and Mathematics (UNSTIM), Abomey 2282 Goho, Department of Zou, Republic of Benin, E-mail: yacets@yahoo.com

Received: 06.05.2025 / Accepted: 21.07.2025 / Revised: 21.08.2025 / Available online: 15.12.2025

DOI: 10.2478/jaes-2025-0022

KEY WORDS: durability, laterite soil, metakaolin, rice husks ash, geopolymer, FEM.

ABSTRACT:

This study examines the performance and the durability of the geocomposite obtained by replacing cement by rice husk ash (RHA)-based geopolymer in stabilizing laterite soil for the use in pavement construction. For that laterite soil was first characterized through tests such as Atterberg limits, compaction test, Californian Bearing Ratio (CBR) and Unconfined Compressive Strength (UCS), and X-ray diffraction. Thermogravimetry (TG) coupled with differential (DTG) and X-ray diffraction analysis showed that the calcination of rice husk power (RHP) at 800°C leaded to amorphous silica needed for the geopolymer synthesis. It was found that the optimum geopolymer formulation 80%MK+20%RHA presents the best physical and mechanical performance, achieving a density of 1.61 t/m^3, a water accessible porosity of 20% and an unconfined compressive strength of 24.6 MPa. The optimum geopolymer formulation was used to stabilize the laterite soil for base layer of pavement. Unconfined compressive strength of geopolymer-stabilized laterite soil is approximately 8% larger than that of cement-stabilized laterite soil. Unconfined tensile strength of geopolymer-stabilized laterite soil is approximately 20% larger than that of cement-stabilized laterite soil. Furthermore, the durability analysis showed that the unconfined compressive strength and the bending strength of geopolymer-stabilized samples decrease up to 70% of the initial compression strength and 75% of the initial bending strength with increasing cyclic wetting-drying, respectively. However, the unconfined compressive strength and the bending strength of geopolymer-stabilized laterite soil are approximately twice those of cement-stabilized laterite soil for a given cyclic number of wetting-drying. The FE simulations of pavement under traffic loading showed that the base layer stabilized with geopolymer and the base layer stabilized with cement present comparable performance regarding the vertical and shear deformation.

Graphic abstract:

1. INTRODUCTION

Infrastructures play fundamental role in the development of nations, and boost economic, social, and environmental prosperity of countries. Their construction and maintenance hold a prominent place in public policies, as illustrated by the case of Benin, where the transportation infrastructures account for more than 25% of the Government Action Program 2021-2026. However, although these construction projects are essential, they face major technical challenges, particularly the low bearing

capacity of the soils used for pavements, which leads to high costs and limits the durability of infrastructures (Elvis et al. 2023).

Soil stabilisation using traditional binders such as cement or lime has long been the preferred solution for improving soil performance. However, this approach has significant limitations, particularly in terms of cost and environmental impact. The cement industry alone was responsible for 8% of global greenhouse gas emissions in 2009 (Habert et al. 2020). CO2 emissions are expected to increase significantly in the coming decades (Humphreys et al. 2002) (Damtoft et al. 2008). If no action is taken, this trend could quadruple by 2050 (Damtoft et al. 2008). Hence, cement production can represent a serious threat to the ecological balance of the planet. Therefore, the questions of exploring alternative, sustainable, and economically viable solutions needed to be solved.

Rice husk ash (RHA) is one of interesting industry by-products for replacing cement due to its pozzolanic properties. Produced from the calcination of rice husks, RHA has a high silica content, reaching approximately 91.37%, which enhances mechanical and chemical properties of RHA stabilised soil (Botchway et al. 2020) (Ahlinhan et al. 2024). The silica in rice husk ash is primarily in amorphous form, making it a reactive material. Indeed, RHA can participate to pozzolanic reaction in the presence of an activator such as calcium hydroxide (lime or cement), leading to the partial substitution of cement by RHA (Elvis et al. 2023), (Nguyen 2020), (Ahlinhan et al. 2024).

In recent years, rice husk ash instead of cement has been widely used in soil stabilization, particularly for laterite soils and clays for reducing greenhouse gas emissions. Soil stabilization is simply a method to improve the properties of soil. There are many methods for soil stabilization, including chemical, physical, mechanical, and thermal techniques. The chemical stabilization of soil, such as laterite, is achieved by adding chemical agents like cement to ensure good grain bonding and improve various soil properties (Ahlinhan et al. 2024). Several studies have obtained interesting results using RHA as a partial substitute for cementitious binders. For instance, (Wibowo et al. 2023) used rice husk ash and pozzolanic cement as additional materials for soil stabilization. Their study concluded that the bearing capacity of the stabilized soil increased compared to the unstabilised soil.

O. Eberemu (2011) studied the consolidation properties of compacted laterite soil treated with rice husk ash. It was observed that the pre-consolidation stress increased with increasing RHA content and that it first decreased before increasing again with higher moisture content. B. Bournebe (2023) used rice husk ash for soil stabilization, and observed that the optimum cement proportion was 8%, and the treated soil's UCS and soaked CBR values increased up to 1.83 MPa and 142%, respectively.

However, despite these promising results, studies on soil stabilization using RHA face limitations when it is used alone due to its low soil improvement potential. Therefore, RHA was sometimes combined with cement (Alhassan 2008). These limitations open the way for the exploration of alternative binders, such as geopolymer binders, which were once widely used in the production of compressed earth bricks (CEB) (Sore et al. 2018), (Ahlinhan et al. 2024). These binders stand out for their ability to produce durable, high-performance materials with low environmental impact. Synthesized from aluminosilicate-rich materials like metakaolin and activated by alkaline solutions, these binders offer a credible alternative to cement while utilizing agricultural waste such as RHA for the stabilization of pavement layers.

This study follows an innovative approach by integrating geopolymer technology, previously used in concrete or CEB manufacturing, into pavement engineering, an area that, remains largely unexplored. The objective of this research is to develop and characterize a geocomposite material derived from the stabilization of laterite soil using RHA- based geopolymer binder, and to assess the performance and the durability of the resulting geocomposite. This material, intended for road base layers, aims not only to improve the mechanical performance and durability of road infrastructure but also to reduce greenhouse gas emissions and associated costs. By focusing on the interaction between laterite soil and the geopolymer binder, as well as the behaviour of the material in its environment, this research contributes to the development of sustainable solutions for road infrastructure in alignment with sustainable development goals.

2. MATERIALS AND METHODS

Materials

The laterite gravel studied in this research was gathered in the department of Zou, specifically in the commune of Djidja, in the district of Mougnon. The geographic coordinates of the site are 7°13'42.92"N (latitude) and 1°59'38.67"E (longitude). The kaolinite clay used for obtaining metakaolin was extracted from a local quarry in Zogbodomey (7.0670° N and 2.33466° E) in the department of Zou in Benin. Table 1 presents the semi-quantitative composition of the clay, which contains 40% kaolinite and 39% quartz (Ahlinhan et al. 2024).

Kaolinite	Quartz	Goethite	Smectite	Illite	Anatase
40%	39%	10%	5%	4%	2%

Table 1. Semi-quantitative composition of the Zogbodomey clay (Ahlinhan et al. 2024)

The data in Table 1 show that the clayey soil from Zogbodomey was mainly composed of kaolinite and quartz. This natural mineralogical composition is favourable for the production of geopolymer binder. The rice husk was collected from the rice husk disposal near the rice factory of Zinvé in the distinct of Abomey-Calavi in Benin. In this factory, the edible rice grains were separated from their husks, which were discarded in the disposal. The collected rice husks were washed to eliminate organic matters and debris. The clean rice husks are then ground into fine particles and passed through 400 mm sieve to obtain the Rice Husk Powder (RHP), that are calcined to obtain the Rice Husk Ash (RHA). Tape water at temperature of about 25°C was used for the experimental tests.

Methods

The laterite soil and the kaolinite clay were firstly characterized. Table 2 presents physical identification and mechanical tests performed for characterizing materials. Additionally, laterite soil sample and rice husk powder were subjected to X-Ray Fluorescence (DRX) test to determine their chemical composition. The test was conducted at research centre SEME CITY in Republic of Benin.

Physical identification tests	Standards applied
Moisture content	NF EN ISO 17892-1 (BS EN ISO 17892-12, 2018)
Particle size distribution	NF EN ISO 17892-4 (EN ISO 17892-10: 2018)
Atterberg limits tests	NF EN ISO 17892-12 (CEN ISO TS 17892-1: 2014)
Methylene-blue absorption test	EN 933-9
Organic matter content	ISO 14235
Proctor compaction test	NF P94-093, 2014
California Bearing Ratio (CBR)	NF P94-078, 2014
Unconfined Compressive Strength (UCS)	ASTM C39/C 39M, 2009

Table 2. Physical identification and mechanical tests performed on materials

Moreover, RHP was subjected to combined thermogravimetry (TG) and differential (DTG) for determining the optimum calcination temperature by which the Rice Husk Ash (RHA) presented amorph chemical compound (no crystalline form of chemical compound), that can react with the chemical compounds of laterite soil and kaolinite. Then, four geopolymers binder with different formulations were synthesised by mixing metakaolin with RHA and activator solution of 12M NaOH. The performance of geopolymer samples of 4cm x 4cm x 16cm were evaluated by means of density, absorption, UCS test for determining the optimum geopolymer formulation.

The laterite soil was stabilized with the optimum geopolymer formulation. The stabilized soil samples were then subjected to compaction, CBR and UCS test for determining the physical and mechanical properties of the geo-composite (laterite soil + geopolymer). For control samples, the laterite soil was further stabilized with Portland cement and the physical and mechanical properties of stabilized soils such as optimum moisture content (OMC), Maximum Dry Density (MDD), California Bearing Ratio (CBR) and Unconfined Compressive Strength (UCS) were determined.

Finally, the performance of geopolymer stabilized laterite samples and cement stabilized laterite samples was compared and evaluated for fulfilling the requirement of road design guideline CEBTP for tropical countries. The graphic abstract presents a simplified graphical illustration of the methodology used for this study.

2.1.1 Syntheses of geopolymer binder with RHA: The metakaolin used for the synthesis of the geopolymer was obtained by calcining local clay at 800°C for 3 hours (10°C/min). Before calcination, the clay was first ground and sieved to 100 µm mesh sieve. The rice husk was also ground and sieved to 100 µm before the calcination. Rice husk ash was obtained by calcining local rice husks powder at 800°C for 4 hours at a temperature rate of 10°C/min.

A 12M sodium hydroxide solution, prepared by dissolving 99% pure NaOH crystals in distilled water, was used as the activation solution for the calcined materials. The synthesis of the geopolymer binder was carried out in two distinct phases.

First, the aluminosilicate ash (metakaolin) and silicate ash (rice husk ash) were carefully mixed and blended in a mixer about 10 minutes until the mix became homogeneous. Then, the alkaline solution NaOH was added, and the mixture of the ashes and the solution was thoroughly homogenized in the mixer for an additional 10 minutes until the mixture became homogeneous. A mass ratio (alkaline solution of NaOH to the ashes (metakaolin + RHA)) of 0.7 was used for the geopolymer synthesis. This ratio of 0.7 resulted from its influence of the physical performance of geopolymer for achieving a consistent geopolymer binder (Sore et al. 2018), (Ahlinhan et al. 2024).

The resulting geopolymer binder was then used to produce geopolymer sample of 4×4×16 cm³. The geopolymer in the mould of 4×4×16 cm³ was subjected to compaction using a vibrating table. The sample in mould underwent 120 impacts to expel air trapped within the geopolymer's pores (Ahlinhan et al. 2024).

Based on the results reported by Ahlinhan et al. (2024) [6], where geopolymer was produced with the same metakaolin but with corn cob ash, it was observed that the strength of geopolymer binders increases with the ash content, reaching 12.08 MPa after 14 days of curing for the formulation of 85% metakaolin and 15% activated ash.

Therefore, the following four formulations of geopolymer binders are synthesized in the present study:
•GB1: 100% metakaolin activated by NaOH solution (12 M)
•GB2: 90% metakaolin and 10% rice husk ash activated by NaOH solution (12 M)
•GB3: 80% metakaolin and 20% rice husk ash activated by NaOH solution (12 M)
•GB4: 70% metakaolin and 30% rice husk ash activated by NaOH solution (12 M)

Once the samples were prepared, they were covered with a polyethylene film to prevent water evaporation during setting and hardening. The samples were left at the laboratory's ambient temperature approximately 30°C for 7 days before undergoing heat treatment at 60°C, in accordance with the studies conducted by Ferone et al. (2011), Ahlinhan et al. (2024). Laterite soil was stabilised with geopolymer binders for improving its physical and mechanical performance in base layer of pavement. Similar methodology was adopted for the control samples, i.e. laterite soil stabilized with cement. Reference is made to (Ahlinhan et al. 2024), (Sore et al. 2018) for details regarding stabilisation process of laterite soil with geopolymer binder and cement.

2.1.2 Durability analysis procedure: To evaluate the durability of geopolymer-treated road foundation materials, the geopolymer-stabilized samples were compacted, subjected to wetting-drying cycles before subjecting to unconfined compressive strength and bending strength. Finally, the test results of geopolymer-stabilized laterite soil were compared to cement-stabilized ones. The test procedure for the durability consists of two main parts: phase of sample compaction and phase of wetting-drying to simulate the wet (flooding) and dry (drought) seasons.

The dynamic compaction of the prepared sample was achieved by a falling mass of 4.5 kg from a height of 45.7 cm corresponding to compaction energy for Proctor test modified, used for compacting the base layer of pavements, The mixture consisting of laterite soil and geopolymer were then compacted in two layers with repeated blows. Initially, the first layer is

formed by filling the 4x4x16 cm³ mould with the mixture and compacting it using the modified Proctor hammer. Scratches and grooves are made on the surface of the first layer to roughen it, enhancing the bond between the first and the second layer. After compaction, each layer has an approximate thickness of 2 cm. The hammer diameter of 5 cm for Proctor test modified is larger than the mould width of 4 cm, so that the hammer cannot enter into the mould for compacting the mixture. To facilitate the compaction and the adapted compacting energy accounting for sample volume and additional metal plate, the blows (12 blows per layer) were applied to the mixture through a metal plate (37 mm width, 157 mm length, and 35 mm thickness) placed onto the sample surface. The metal plate is divided into three sections with specific compaction patterns, as shown in 3 and 4. After the compaction, the stabilized samples are wrapped in plastic film and cured for 28 days before being subjected to wetting-drying cycles.

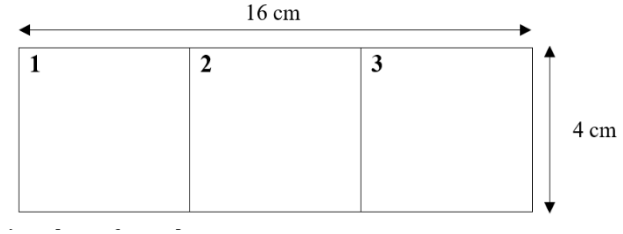

Figure 3. Compaction plane of sample

Figure 4. Sample compaction: modified Proctor hammer (A), metal plate (B) 3xmould 4x4x16 cm³

In this study, the wetting-drying cycle test was carried out following the procedure described in Abbey et al. (2023), ASTM D559/D559M-15 (2016). After curing the samples, the plastic film was removed from the samples, and they were wrapped with adhesive tape, leaving the top and bottom exposed. This was done to keep the sample intact as a single piece during the wetting-drying cycles. All samples were immersed in water for 5 hours at an ambient temperature of 20 ± 2 °C to simulate flooding during heavy rainfall.

After the 5-hour soaking period, the samples were removed, weighed, and their mass was recorded for monitoring mass variations throughout the cycles. Following the soaking phase, six samples were set aside, three samples were tested for unconfined compressive strength (UCS) and three samples were tested for bending strength (wetting cycle No. 1).

The remaining soaked samples were then placed in an oven at a temperature of 71 ± 3 °C for 42 hours to simulate extreme drought conditions or high temperatures. After 42 hours, the dry samples were taken out, and their masses were recorded. Next, six samples were set aside, three tested for unconfined compressive strength (UCS), and three tested for bending strength (drying cycle No. 1).

This procedure constitutes one wetting-drying cycle (48 hours). The process was repeated until 12 cycles were completed to assess the effect of wetting-drying cycles on the durability of the treated foundation layers for pavement. To evaluate the durability of geopolymer-treated road foundation materials, the geopolymer-stabilized samples were compacted, subjected to wetting-drying cycles before subjecting to unconfined compressive strength and bending strength. Finally, the test results of geopolymer-stabilized laterite soil were compared to cement-stabilized ones. The test procedure for the durability consists of two main parts: phase of sample compaction and phase of wetting-drying to simulate the wet (flooding) and dry (drought) seasons.

2.1.3 Simulation and modelling: A three-dimensional finite element model of a pavement system consisting of surface layer, base layer stabilised with geopolymer, sub-base layer and natural soil has been developed and analysed. The finite element programme Abaqus 3D CAE Version, 2021 has been used for the simulations. In order to reduce computational effort, only one half of the pavement structure was modelled. Preliminary analyses have been carried out for determining the model geometry and the mesh size in order to reach sufficient accuracy of the results and to avoid the influence of the boundary conditions. These analyses lead to model with width of 3 m, length of 3 m and depth of 2 m. A mesh based on C3D8 (8-knot volume elements) elements available in the Abaqus 3D has been applied. The elastic behaviour is considered for the different layers of the pavement. A static load was applied to at the centre of the FE model. This load was applied perpendicularly to equivalent surface of the pavement, approximately corresponding to the footprint of a truck tire (Hadi et al. 2003). The load used in this analysis is 3.25 tons, representing the load on one wheel of a standard 13-ton tandem axle load. Fixed boundary conditions are applied at the corner and bottom of the model. The parallel faces to the z-axis is blocked in the direction of the x-axis, and the model is fixed at the bottom (Wang et al. 2021).

3. RESULTS AND DISCUSSIONS

Physical and chemical analysis of raw materials

3.1.1 Physical analysis: Figure 5 presents the curves of grain size distribution for the laterite soil and clay used. The soil consists of wide graded clayey and silty sand with about 20% of gravel. The soil classification in accordance with NF EN ISO 17892-4, (EN ISO 17892-10: 2018) shows that the laterite soil tested is of class B5. The grain size distribution curves lie within the lower and upper bound curves for the base layer specified by the road guideline CEBTP. Therefore, the laterite soils tested can be used for base layer of pavement regarding the grading point of view.

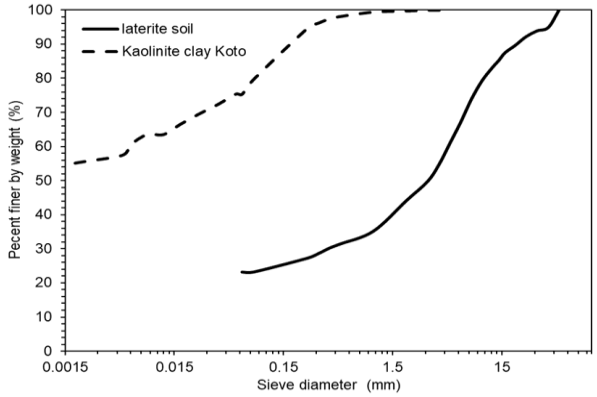

Figure 5. Grain size distribution curve of laterite soil and kaolinite clay

Based on the particle size distribution shown in Figure 5, the laterite soil contains approximately 20% gravel, 60% sand, 10% silt and 10% clay. Atterberg limits tests showed a liquid limit of 31.25 % and plasticity index of 12.25% of the laterite soil. For obtaining the metakaolin, the kaolinite clay was used. The clay is characterised with a liquid limit of 70% and a plasticity index of 30%, so that this clay can potentially experience a high swelling. The results of Proctor compaction test for the laterite soil showed optimum water content of 10% with corresponding maximum dry density of 2.27 t/m^3.

3.1.2 Thermogravimetry (TG) and differential (DTG) analysis: For the determination of the optimum calcination temperature for mobilizing amorphous silica, RHP was subjected to combined thermogravimetry (TG) and differential (DTG). Figure 6 shows the curves of the thermal degradation characteristics of RHP at a heating rate of 10°C/min. The decarbonation process of the lignocellulosic biomass can be divided into three main regions: moisture and very light volatiles components removal (< 120°C); degradation of hemicellulose (220–315°C); lignin and cellulose decomposition (315–400°C) and lignin degradation (> 450°C) (Sanchez-Silva et al 2012), (Yang et al 2007). The loss of lignin typically occurs at a slower rate over a much wide temperature range of 180–900°C.

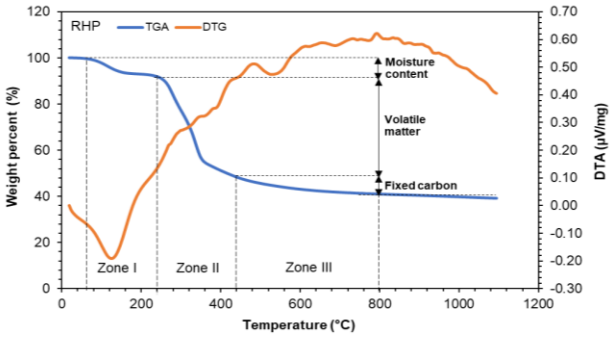

Figure 6. Thermo-gravimetric analysis (TGA) and differential thermal analysis (DTA) curves for RHP

As shown in figure 6, the moisture loss and very light volatiles components removal is followed by the second region of weight loss, i.e. devolatilization, at 240°C for rice husk powder. Much of the devolatilization occurred in the second region of weight loss, a result of the thermal breaking of weak bonds in the polymeric structure of the constituent components of the biomass and the formation of stronger, more stable bonds to take place (Roque-Diaz et al. 1985). Lignocellulosic biomasses such as rice husks are known to contain hemicelluloses, cellulose and lignin. The devolatilization region should correspond mainly to the degradation of these components (Biagini et al. 2006). On the DTG curves the temperatures at which maximum rate of weight loss occurred are described by the position of the peaks in the curve. The DTG curve of the rice husk materials during the devolatilization stage shows a peak (after which is represented by a noticeable change in slope of the TG curve). Based on the temperature range at which cellulose, hemicelluloses and lignin have been previously observed to decompose, the DTG peaks of rice husks powder can be assigned as follow: The first DTG peak at 120°C is probably due to the decomposition of hemicelluloses and the second peak at 440°C is due to cellulose. Hereby, the first and second peak are well distinct, that can be explained with high about 20% of ash content of RHP (Antal and Varhegyi 1995).

The third region sees a much lower rate of weight loss than the second stage. This region of biomass decomposition corresponds to the end of cellulose decomposition, and the degradation of heavier volatiles, the cracking of C–C bonds and the formation of amorphous silica with high pozzolanic activity. For temperature larger than 800°C, crystalline quartz showing poor reaction activity with other chemical compounds will be formed. Therefore, the decarbonation of rice husks powder was carried out at 800°C.

3.1.3 X-ray diffraction (to be improved regarding analysis DRX soil and RHA): The result of X-ray diffraction for laterite soil is shown in figure 7. The diffractogram indicated that the main chemical compounds (minerals) of the laterite soil are silicate oxide (quartz), aluminium oxide (alumina) and iron oxide (iron). With the EVA software, the relative abundance of each identified mineral was estimated semi quantitatively considering the net area of the peaks in the diffraction pattern (Table 8). The diffractogram of RHA indicated that quartz is the main mineral of RHA (figure 9), and the percent of the minerals is given in Table 8. These mineral phases are those commonly present in laterite soil reported in (Sore et al. 2008), (Millogo et al. 2008), (Ahlinhan et al. 2024).

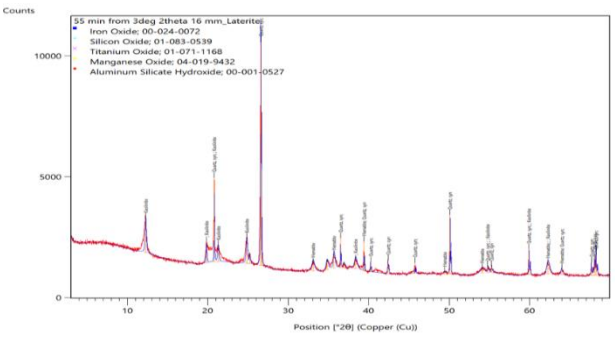

Figure 7. X-Ray diffraction of laterite soil

¤	Physical·tests¤		Chemical·compositions·(%)¤									
¤	Specific·gravity·(g/cm^3)¤	Blaine¶ (cm^3/g¤	SiO_2¤	Al_2O_3¤	Ti_2O¤	Fe_2O_3¤	CaO¤	MgO¤	Na_2O¤	MnO¤	K_2O¤	LOI¤
Laterite¤	2.02¤	-¤	45.1¤	20.1¤	2.3¤	11.6¤	0.08¤	0.10¤	0.01¤	0.01¤	0.21¤	-¤
Clay·calcined¤	¤	¤	52.0¤	43.8¤	1.5¤	0.3¤	-¤	-¤	0.3¤	-¤	0.1¤	-¤
Cement¤	3.21¤	3200¤	19.8¤	7.1¤	-¤	3.6¤	56.2¤	1.2¤	0.38¤	-¤	0.69¤	0.06¤
RHA¤	1.95¤	3600¤	89.61¤	0.04¤	-¤	0.22¤	0.91¤	0.42¤	0.07¤	-¤	1.58¤	5.91¤

Table 8. Physical and chemical properties of laterite soil, calcined clay, cement and RHA

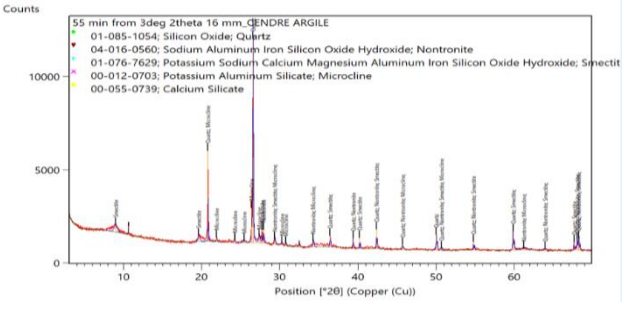

Figure 9. X-Ray diffraction of calcined kaolinite clay

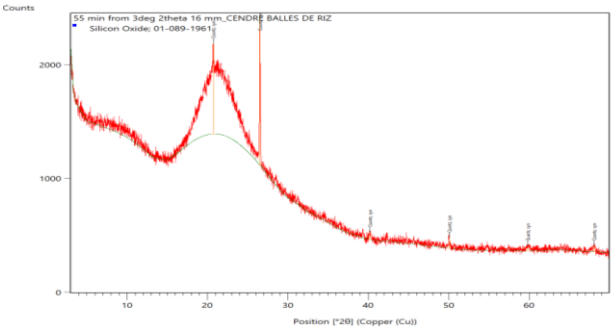

Figure 10. X-Ray Diffraction of RHA

Physical behaviour of geopolymer

The mass loss, the apparent density, the water-accessible porosity, and the compressive strengths of RHA-based geopolymer binders are presented in this section, and compared to those of CCA-based geopolymer reported in (Ahlinhan et al. 2024). Figure 10 presents the mass loss of different geopolymer binder samples after thermal curing at 60°C for 7 days. Mass loss of 21.29%, 21.07%, 14.38%, and 12.01% were determined for binders GB1, GB2, GB3 and GB4, respectively. This mass loss is attributed to the evaporation of water from the alkaline solution (figure 11). Similar results were reported by Sore et al. (2018) for RHA-based geopolymer and by Ahlinhan et al. (2024) for CCA-based geopolymer.

Furthermore, the mass loss decreases as the partial substitution of calcined clay and rice husk ash increases. This reduction can be explained by the fact that the silica in rice husk ash is less soluble in hot water than in cold water. Consequently, this silica migrates out of the geopolymer during thermal curing, reducing the geopolymer porosity and limiting the amount of water that can be trapped inside (Ahlinhan et al. 2024). The addition of rice husk ash to metakaolin generally increased the amount of amorphous silica in the aluminosilicate mixture. This likely enhanced the release of silicate ($SiO(OH)_3$) compounds during the alkaline hydrolysis dissolution stage, and improves the performance of geopolymer. Figure 12 presents the apparent density and water-accessible porosity of geopolymer binders cured at 60°C.

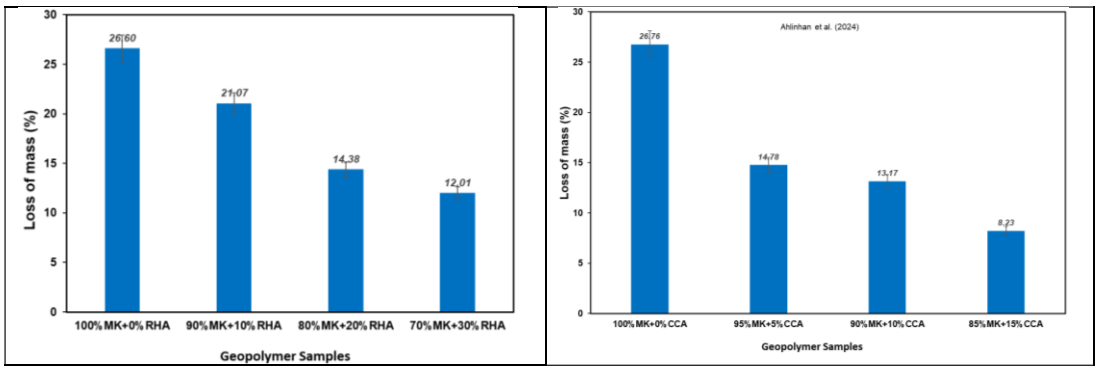

Figure 11. Mass loss of geopolymer samples (insert results of geopolymer)

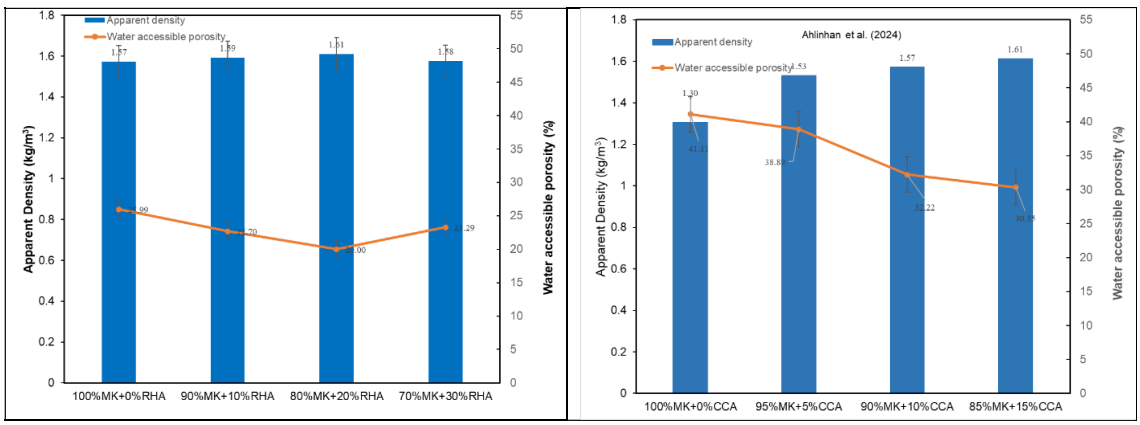

Figure 12. Apparent density and water accessible porosity of geopolymers

In general, the density increases and the porosity decreases with increasing RHA or CCA content. Apparent density ranges from 1.57 to 1.61 t/m^3, with the maximum density achieved by GB3 (80%MK+20%RHA). This maximum density can be attributed to gelation and good condensation of the geopolymer gel at the curing temperature, as well as the more developed geopolymer phase. However, the lower density for samples GB1, GB2 and GB4 is likely due to slower dissolution of raw materials and

slower gel condensation, leading to lower density and higher porosity. This higher density of the GB3 sample can lead to large strength (Ahlinhan et al. 2024). The apparent density of the three types of geopolymer samples (GB1, GB2 and GB4) presented in this study are slightly lower than those obtained by Gao et al. (2013), Sore et al. (2018). The porosity ranges from 20% to 25.99%, while the density ranges from 1.57 to 1.61.

Mechanical performance of geopolymer

The compressive strengths of the geopolymers produced with metakaolin, RHA and NaOH, are shown in figure 13. Geopolymers GB3 (80%MK+20%RHA) exhibit compressive strengths of 24.60 MPa higher than those of the samples of GB1, GB2, GB4). This result can be linked to the high density of the geopolymer binders (LG3) as shown earlier. These results are consistent with those reported by Sore et al. (2020), Ahlinhan et al. (2024).

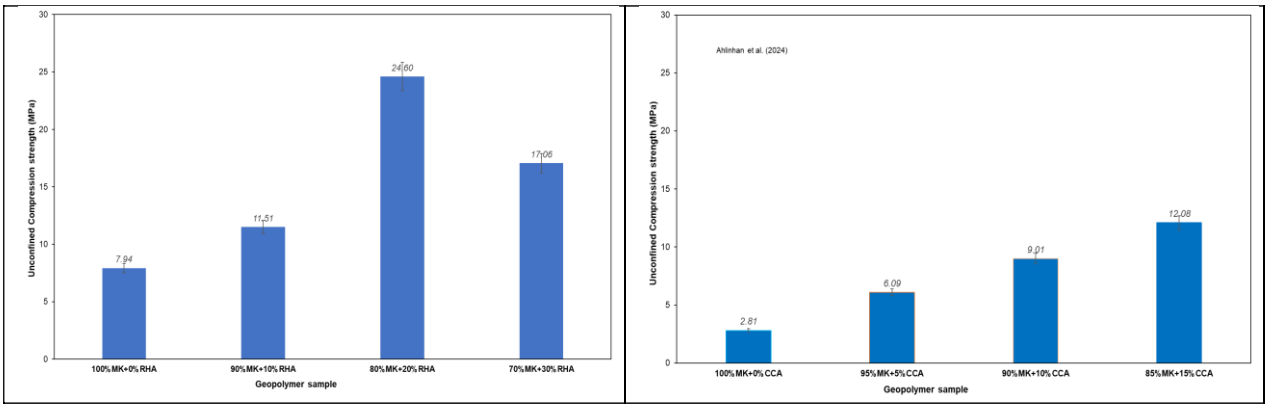

Figure 13. UCS of geopolymer after 14 days of curing

The improvement in mechanical strengths of geopolymers produced with metakaolin, RHA and NaOH is in line with the findings by (Duxson et al. (2007), (Sore et al. 2020). The increased compressive performance of NaOH-based samples can be attributed to a greater dissolution of aluminosilicates in the presence of sodium hydroxide solution (Xu and Deventer 2000), (Sore et al. 2020). The studies argued that the smaller ionic size of Na+ promotes the formation of ion pairs with smaller silicate oligomers, improving the bond and the cohesion between particles.

Furthermore, it is important to note that the mechanical properties of geopolymer binders were improved in proportion to the amount of rice husk ash (RHA). It was found that this improvement in strength reaches a maximum for sample GB3 (80%MK+20%RHA), achieving 24.6 MPa, before decreasing to 17.06 MPa by 30% RHA. The incorporation of rice husk ash increases the amount of amorphous silica in the complex aluminosilicate mixture. That facilitates the release of silicate species such as [$SiO(OH)_3$] during the alkaline hydrolysis dissolution phase. This incorporation leads to an improvement in the mechanical properties of the geopolymer binders (Ahlinhan et al. 2024), (Pacheco-Torgal 2008). The high concentration (12M) of the alkaline solution used, induces the formation of a gel composed of an extensive three-dimensional aluminosilicate network that plays a key role in the bonding between particles, allowing them to withstand stresses such as compression.

Despite the improvement in the mechanical properties of geopolymer binders with the addition of RHA, it is important to note that these properties remain almost lower than those reported by Zhang et al (2014), Pelisser et al (2013) (20 to 70 MPa). This difference can be explained by the water/solid mass ratio of 0.7 used during geopolymer synthesis, as well as the low apparent densities of the samples, which could contribute to these more modest mechanical strengths compared to the results reported by these researchers. However, the mechanical performance of the geopolymer binder GB3 with unconfined compressive strength of 24.6 MPa fulfils the requirement of road design guideline (CEBTP) to be used for stabilizing laterite soil for base layer of pavements.

In summary, the results of this study highlight the influence of rice husk ash incorporation on the characteristics of geopolymer binders. The thermal curing of geopolymer binders accelerates the dissolution of silicate compounds during the geopolymerization reaction, although it leads to mass loss due to evaporation of water from the alkaline solution. This significant evaporation can promote the formation of micro voids, making the samples more porous and less dense, particularly for the GB1 and GB2 samples.

Additionally, thermal curing improves the compressive strength of geopolymer binders. The partial substitution of calcined clay with rice husk ash promotes the development of the amorphous phase at the expense of mineral crystallinity, resulting in significant improvement in mechanical strength. This improvement reaches a maximum when the proportion of rice husk ash reaches 20% for samples GB3 before subsequently decreasing to 17.06% at 30%RHA. Therefore, the formulation GB3 (80%MK+20%RHA) is considered for stabilizing laterite soil, to obtain the geocomposite for using in pavement structure, due to its excellent physical and mechanical properties.

The CBR index of raw laterite soil is significantly lower than that of the cement-stabilized and geopolymer-stabilized laterite soil (Figure 14). However, CBR index of cement-stabilized laterite soil is almost larger than that of geopolymer-stabilized laterite soil. That can be explained with the different curing condition of cement as hydraulic binder, and geopolymer binder as thermal binder. Indeed, the CBR test requires the curing of the sample in water, that strengthen the mechanical performance of cement-stabilized soil. However, geopolymer is a thermal binder, therefore geopolymer-stabilized soil needs thermal curing for

boosting its mechanical performance. CBR value is above 160%, the geocomposite (geopolymer stabilised laterite soil) can be used for base layer of pavement according to the road design CEBTP guideline.

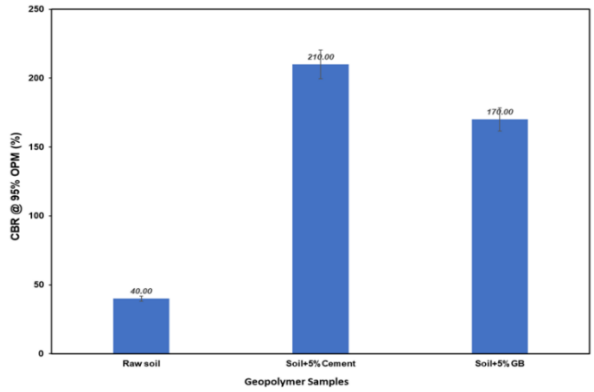

Figure 14. CBR index of laterite soil stabilized with cement and geopolymer binder

An optimum cement content of 5% by dried weight of mix was assessed for the laterite soil studied, based on the results of optimum water content, CBR and UCS of cement stabilized laterite soil. Figure 15 presents unconfined compressive and tensile strength of both cement- and geopolymer-stabilized laterite soil. Unconfined compressive strength of geopolymer-stabilized laterite soil is approximately 8% larger than that of cement-stabilized laterite soil. Unconfined tensile strength of geopolymer-stabilized laterite soil is approximately 20% larger than that of cement-stabilized laterite soil. Since, CBR value and UCS value are larger than those required by road design guideline (CBR sup 160%, UCS 1.8-3 MPa), then the formulated geopolymer binder based on local bio-sourced materials can be used for base layer of pavement construction.

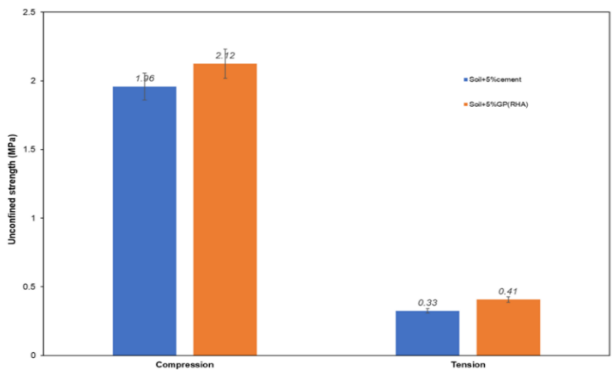

Figure 15. Comparison of unconfined strength

Durability of RHA-geopolymer stabilized laterite soil

The values of unconfined compressive strength (UCS) and the bending strength presented in this section was the average value of three samples to ensure validity and accuracy of the results. Figure 16 presents the unconfined compressive strengths of the geopolymer-stabilized laterite soil and cement-stabilized laterite soil depending on cyclic numbers of wetting-drying.

Figure 15 illustrates the comparison of the different mechanical strengths obtained.

The unconfined compressive strengths decrease with increasing number of cycles. The observations confirm the findings by (Abbey et al. 2023), (Hu et al. 2019) for clayey materials subjected to cyclic wetting-drying. For the geopolymer-stabilized samples, the unconfined compressive strength decreases from 15 MPa for cyclic number of 1 to 4 MPa for cyclic number of 12, corresponding to an approximated 70% reduction in the initial compression strength. For cement-stabilized samples an approximated 85% reduction in the initial compression strength was observed.

The decrease of the unconfined compressive strength can be attributed to cyclic swelling-shrinking of clay minerals in laterite soil due to repeated wetting-drying, resulting in weakening of the binder strength within the samples. For geopolymer-stabilized samples, the unconfined compressive strength in wetting phase is generally larger than that in drying phase. However, the unconfined compressive strength of cement-stabilized laterite soil for wetting phase is smaller than that for drying phase for number of cycles ranging from 1 to 3, above which the compressive strength for wetting phase is larger than that for drying phase.

The unconfined compressive strength of geopolymer-stabilized laterite soil is larger than that of the cement-stabilized laterite soil. The unconfined compressive strength of geopolymer-stabilized laterite soil is approximately twice that of the cement-stabilized laterite soil. This can be explained with high compressive strength of 25 MPa of the RHA-geopolymer synthetised (see figure 13).

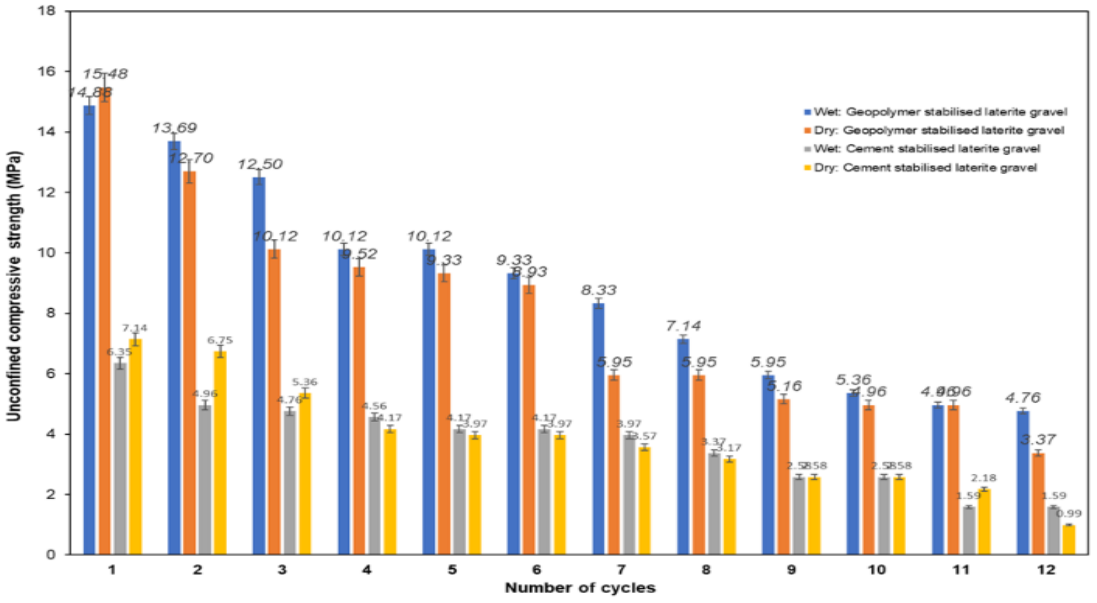

Figure 16. Unconfined compressive strength with number of cycles

Like the unconfined compressive strength, the bending strength of both RHA-geopolymer stabilized laterite soil and cement stabilized laterite soil decreases with increasing number of cyclic wetting-drying (figure 17). For a given number of cycles, the bending strength of the RHA-stabilized geopolymer in wetting phase is generally slightly larger than that of RHA-stabilized geopolymer in drying phase. For cement-stabilized laterite soil, the bending strength in wetting phase and the bending strength in wetting phase showed insignificant difference. For the geopolymer-stabilized samples, the bending strength decreases from 2.8 MPa for cyclic number of 1 to 0.7 MPa for cyclic number of 12, corresponding to an approximated 75% reduction in the initial bending strength. For cement-stabilized samples an approximated 70% reduction in the initial bending strength was observed (figure 17). The bending strength of RHA-geopolymer stabilized laterite soil is larger than that of the cement-stabilized laterite soil. The bending strength of RHA-geopolymer stabilized laterite soil is approximately twice of that the cement-stabilized laterite soil for a given number of cyclic wetting-drying (figure 17).

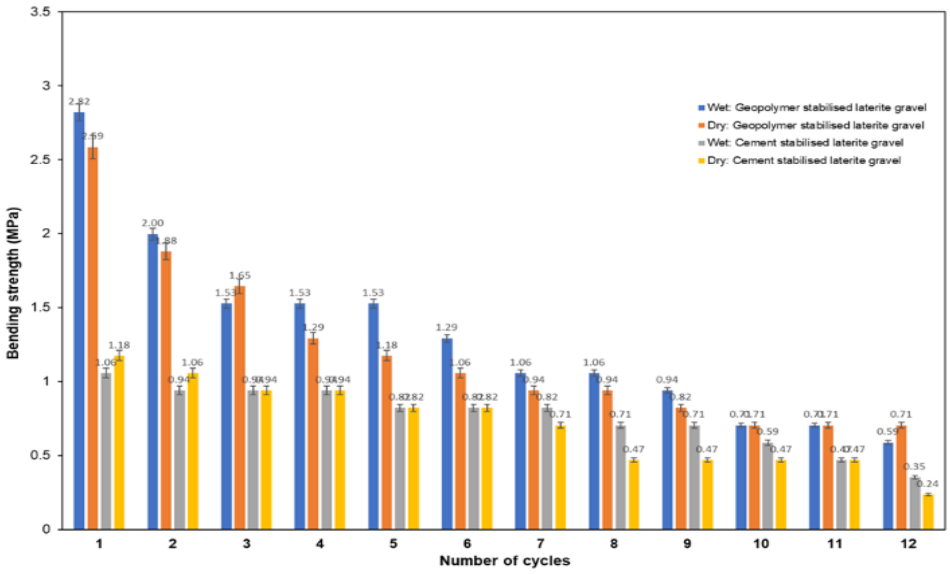

Figure 17. Bending strength with number of cycles

Results of modelling and simulation

Figure 18 shows the finite element model generated in Abaqus software.

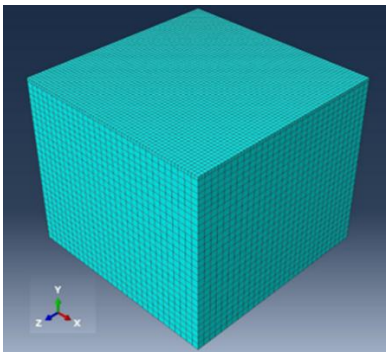

Figure 18. Meshing of the Model

The response of asphalt pavements under loading conditions can be assessed through the deflection at the pavement surface, the horizontal tensile displacement at the bottom of the base layer (Ferone 2011). Table 19 presents the inputs parameters of numerical model, that are derived to some extent from the laboratory tests.

Pavement layers	Modulus E (MPa)	Poisson's Ratio ν	Thickness e (mm)	Density ρ (kg/m³)
Surface Layer	1180	0.35	50	2400
Base Layer	LG: 3461	0.25	150	LG: 2110
	LC: 3057			LC: 2100
Sub-base Layer	200	0.35	250	2170
Natural Soil	100	0.35	∞	1600

Table 19. Input material properties for FE model

Figure 20 shows the deformation of the numerical model subjected to traffic loading.

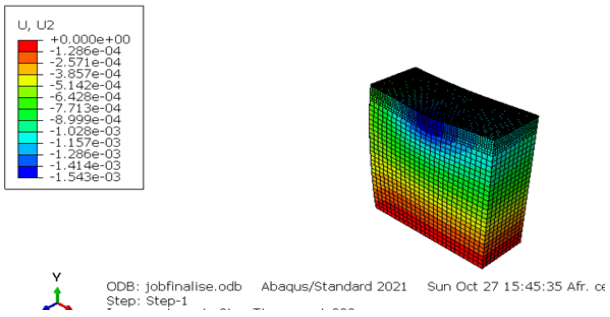

Figure 20. Displacement for number of cycle N=0

Figure 21 represents the deflection at the surface of the pavement whose base layer was stabilized with geopolymer. The shading shows the variations in deflection, with a maximum deflection of 1.700×10^{-4} m at the point of load application.

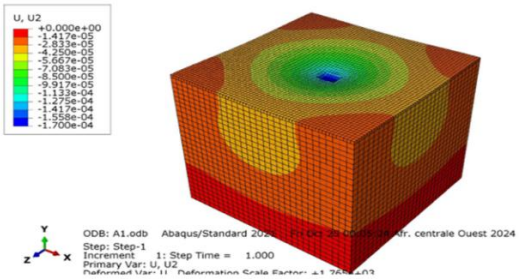

Figure 21. Mesh deformation showing surface deflection of the geopolymer stabilized pavement base layer

Figure 22 presents the numerical vertical displacements of pavement surface whose base layer stabilized with geopolymer, and stabilized with cement. Both curves exhibit a "V" shape, with maximum deflection at the centre, as expected. For the cement-stabilized soil for pavement base, the deflection is slightly higher than those of the geocomposite, with values of 0.18 m and 0.17 m, respectively.

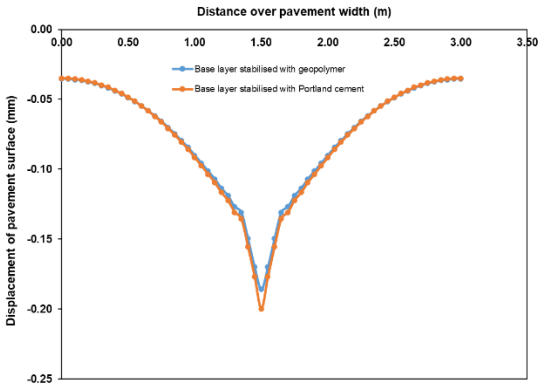

Figure 22. Comparison of deflection values at pavement surface

That demonstrates the comparable performance of both binders used in stabilizing laterite soil in pavement layers.
Figure23 shows a slight difference in performance regarding the tensile deformation at the bottom of base layer. That confirms the comparable performance of geopolymer-stabilized und cement-stabilized laterite soil for pavement layer.

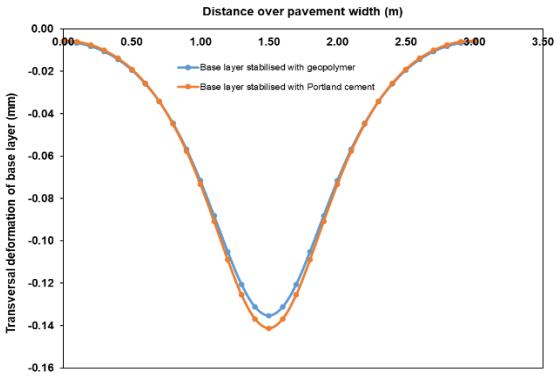

Figure 23. Comparison of maximum tensile strain values at bottom of base layer

4. CONCLUSIONS

The laterite soil in this study consisting of clayey sand was categorized B5 in accordance with NF EN ISO 17892-4, (EN ISO 17892-10: 2018 classification system. The chemical analysis shows that the main chemical compounds of the laterite soils are silicate oxide (quartz), aluminium oxide (alumina) and iron oxide (iron). According to X-ray diffraction, rice husk powder contains mainly silicate oxide (SiO2) and was classed as pozzolanic material.

Combined thermogravimetry (TG) and differential (DTG) analysis on rice husk powder revealed mass loss during the moisture release for temperature range from 50°C to 240°C, followed by release of volatile matter from 240°C to 400°C. The release of fixed carbon was found to occur from 400°C to 800°C. Hence, the decarbonisation of rice husk powder for mobilizing the amorphous silica necessary for high mechanical performance is established to be 800°C.

RHA-based geopolymers have been synthesised by substituting metakaolin with RHA (0, 10, 20 and 30%). It was found that the optimum geopolymer formulation 80%MK+20%RHA presents the best physical and mechanical performance, achieving a density of 1.61, a water accessible porosity of 20% and a compression strength of 24.6 MPa.

The optimum geopolymer formulation was used to stabilise the laterite soil for base layer of pavement. Unconfined compressive strength of geopolymer-stabilized laterite soil is approximately 8% larger than that of cement-stabilized laterite soil. Unconfined tensile strength of geopolymer-stabilized laterite soil is approximately 20% larger than that of cement-stabilized laterite soil. CBR value of 170% and UCS value of 2.12 MPa are larger than those required by road design guideline (CBR sup 160%, UCS 1.8 – 3.0 MPa), hence the formulated geopolymer binder based on local bio-sourced materials can be used for base layer of pavement construction.

The unconfined compressive strength and the bending strength of stabilized laterite soil subjected to cyclic wetting-drying decrease with increasing cyclic wetting-drying. For the geopolymer-stabilized samples, the unconfined compressive strength and the bending strength decreases up to 70% of the initial compression strength and 75% of the initial bending strength, respectively. The unconfined compressive strength and the bending strength of geopolymer-stabilized laterite soil are approximately twice those of cement-stabilized laterite soil for a given cyclic number of wetting-drying.

The FE simulations of pavement under traffic loading shows that the base layer stabilized with geopolymer and the base layer stabilized with cement present similar performance regarding the vertical and shear deformation. Hence, it can be concluded that RHA-based geopolymer is an ideal material that can replace cement in the process of laterite soil stabilization for pavement construction purposes for reducing the greenhouse gases.

Data availability: The data that support the findings of this study are available from the corresponding author upon reasonable request.

Acknowledgments: The authors gratefully acknowledge the financial support received for this work from the UNSTIM Competitive Funds, 2023 edition of the National University of Science, Technology, Engineering, and Mathematics (UNSTIM).

References

I. U. Elvis and I. C. Chinwuba, “Optimization of the California Bearing Ratio of Lateritic Soil Stabilized with Rice Husk Ash using Scheffe’s Method,” J. Kejuruter., vol. 35, no. 3, pp. 705–715, 2023, doi: 10.17576/jkukm-2023-35(3)-19.

G. Habert, S. A. Miller, V. M. John, J. L. Provis, A. Favier, A. Horvath & K. L. Scrivener, “Environmental impacts and decarbonization strategies in the cement and concrete industries,” Nat Rev Earth Environ 1, 559–573 (2020). https://doi.org/10.1038/s43017-020-0093-3.

J. S. Damtoft, J. Lukasik, D. Herfort, D. Sorrentino, and E. M. Gartner, “Sustainable Development and Climate Change Initiatives” Cement and Concrete Research, 38, 115-127, 2008, http://dx.doi.org/10.1016/j.cemconres.2007.09.008.

D.N.-L. Botchway, R.O. Afrifa, C.Y. Henaku, (2020) Effect of Partial Replacement of Ordinary Port land Cement (OPC) with Ghanaian Rice Husk Ash (RHA) on the Compressive Strength of Concrete. Open Journal of Civil Engineering, 10, 353-363. https://doi.org/10.4236/ojce.2020.104027.

D. T. Nguyen, N. T. Nguyen, H. Ngoc, T. Pham, H. H. Phung, and H. Van, “Rice husk ash and its utilization in soil improvement: An overview” Journal of Mining and Earth Sciences Vol. 61, Issue 3 (2020) 1 - 11.

M. F. Ahlinhan, E. Chabi, F. Sedoka, A. Akponon, and E. C. Adjovi, “Synthesis and Characterization of Local Bio-Sourced Geopolymer Binder: Application to Compressed Earth Blocs,” vol. 14, pp. 49–60, 2024, doi: 10.17265/2161-6213/2024.4-6.002.

D. E. Wibowo, M. Endaryanta, and H. Prayuda (2023) “Soil stabilization using rice husk ash and cement for pavement subgrade materials” Revista de la Construcción. Journal of Construction, 22(1), 192-202. https://doi.org/10.7764/RDLC.22.1.192.

E. A. Eberemu (2011) “Consolidation Properties of Compacted Lateritic Soil Treated with Rice Husk Ash” Geomaterials, 2011, 1, 70-78 doi:10.4236/gm.2011.13011.

Bournebe B., Onchiri R.O, Thuo J. Ng. (2023), Investigation on the Suitability of High Clay Lateritic Soils Stabilized with Cement and Rice Husk Ash for Use in Road Base Construction: A Case Study of Juja Town, nternational Journal of Engineering Trends and Technology, https://doi.org/10.14445/22315381/IJETT-V71I2P215.

Alhassan, M. (2008) “Potentials of Rice Husk Ash for Soil Stabilization”. Assumption University (AU) Journal of Technology, 11, 246 -250. http://repository.futminna.edu.ng:8080/jspui/handle/123456789/2256.

S. O. Sore, A. Messan, E. Prud’homme, G. Escadeillas, and F. Tsobnang, “Synthesis and characterization of geopolymer binders based on local materials from Burkina Faso – Metakaolin and rice husk ash,” Constr. Build. Mater., vol. 124, pp. 301–311, 2018, https://doi.org/10.1016/j.conbuildmat.2018.01.051.

M. N.S. Hadi, B.C. Bodhinayake (2003) “Non-linear finite element analysis of flexible pavements”, Advances in Engineering Software 34 (2003) 657–662, doi:10.1016/S0965-9978(03)00109-1.

E. U. Nathaniel, N. J. George, J. I. Ibanga, and A. M. Ekanem, “Efficacy of Hilbert-Huang Transform (HHT) in the Analysis of Instantaneous Low Frequency Waves of Magnetosheath,” Int. J. Geosci., vol. 07, no. 01, pp. 11–19, 2016, doi: 10.4236/ijg.2016.71002.

H. Wang, J. Yang, and H. Wang, "Numerical Simulation on Reflective Cracking Behavior of Asphalt Pavement" Appl. Sci. 2021, 11, 7990. https://doi.org/10.3390/ app11177990.

A. Nega, D. Gedafa, and H. Nikraz, "Stress and Strain Characteristics in Flexible Pavement Using Three-Dimensional Nonlinear Finite Element Analysis," Int. J. Pavement Res. Technol., no. 0123456789, 2024, doi: 10.1007/s42947-024-00422-2.

Y. Lokesh, H. R. Parate, H. M. R. Swamy, and H. Ali, "Development of prediction model for structural behavior and gradation of porous asphalt pavement," Discov. Civ. Eng., vol. 1, no. 1, 2024, doi: 10.1007/s44290-024-00012-y.

K. Gao et al., "Effect of nano-SiO2 on the alkali-activated characteristics of metakaolin-based geopolymers," Constr. Build. Mater., vol. 48, pp. 441–447, 2013, doi: 10.1016/j.conbuildmat.2013.07.027.

P. Duxson, S. W. Mallicoat, G. C. Lukey, W. M. Kriven, and J. S. J. van Deventer, "The effect of alkali and Si/Al ratio on the development of mechanical properties of metakaolin-based geopolymers," Colloids Surfaces A Physicochem. Eng. Asp., vol. 292, no. 1, pp. 8–20, 2007, doi: 10.1016/j.colsurfa.2006.05.044.

H. Xu and J. S. J. Van Deventer, "The geopolymerisation of alumino-silicate minerals," Int. J. Miner. Process., vol. 59, no. 3, pp. 247–266, 2000, doi: 10.1016/S0301-7516(99)00074-5.

F. Pacheco-Torgal, J. Castro-Gomes, and S. Jalali, "Alkali-activated binders: A review. Part 2. About materials and binders manufacture," Constr. Build. Mater., vol. 22, no. 7, pp. 1315–1322, 2008, doi: 10.1016/j.conbuildmat.2007.03.019.

Z. Zhang, H. Wang, Y. Zhu, A. Reid, J. L. Provis, and F. Bullen, "Using fly ash to partially substitute metakaolin in geopolymer synthesis," Appl. Clay Sci., vol. 88–89, pp. 194–201, 2014, doi: 10.1016/j.clay.2013.12.025.

F. Pelisser, E. L. Guerrino, M. Menger, M. D. Michel, and J. A. Labrincha, "Micromechanical characterization of metakaolin-based geopolymers," Constr. Build. Mater., vol. 49, pp. 547–553, 2013, doi: 10.1016/j.conbuildmat.2013.08.081.

Asociación Mundial de la Carretera., REVUE du guide pratique de dimmensionement des chaussées pour les pays tropicaux. 2019.

A. Dione, "Estimation du Module réversible de Graves Non traitées et modélisation par éléments finis de chaussées souples en vue d'un dimensionnement mécanistique-empirique", doi: 10.13140/RG.2.1.4847.8961.

C. Ferone, F. Colangelo, R. Cioffi, F. Montagnaro, L. Santoro, "Mechanical performances of weathered coal fly ash based geopolymer bricks" Procedia Eng., vol. 21, pp. 745–752, 2011, doi: 10.1016/j.proeng.2011.11.2073.

I. Blanco, A. D'Angelo, V. Viola, L. Vertuccio. M. Catauro "Metakaolin-based geopolymers filled with volcanic fly ashes: FT-IR, thermal characterization, and antibacterial property", Science and Engineering of Composite Materials 2023; 30: 20220192, https://doi.org/10.1515/secm-2022-0192.

Sore, S.O., Messan, A., Prud'Homme, E., Escadeillas, G. and Tsobnang, F. (2020) Comparative Study on Geopolymer Binders Based on Two Alka line Solutions (NaOH and KOH). Journal of Minerals and Materials Characterization and Engineering, 8, 407-420. https://doi.org/10.4236/jmmce.2020.86026.

Simulia (2021) Abaqus User's manual, version 6.18. Simulia, Providence, RI, USA.

K. Humphreys, M. Mahasenan, Toward a sustainable cement industry. Sub-study 8: climate change, An Independent Study Commissioned to Battelle by World Business Council for Sustainable Development, March 2002.

C.E.B.T.P Guide pratique de dimensionnement des chaussées pour les pays tropicaux, 1984, 147 pages.

Sanchez-Silva L, Lopez-Gonzalez D, Villasenor J, Sanchez P, Valverde JL. Thermogravimetric–mass spectrometric analysis of lignocellulosic and marine biomass pyrolysis. Bioresour. Technol. 2012; 109:163–72.

Yang H, Yan R, Chen H, Lee DH, Zheng C. Characteristics of hemicellulose, cellulose and lignin pyrolysis. Fuel 2007, 86:1781–8.

Roque-Diaz P, University C, Villas L, Shemet CVZh, Lavrenko VA, Khristich VA. Studies on thermal decomposition and combustion mechanism of bagasse under non-isothermal conditions. Thermochim Acta 1985, 93:349–52.

Biagini E, Barontini F, Tognotti L. Devolatilization of biomass fuels and biomass components studied by TG/FTIR technique. Ind Eng Chem Res 2006;45: 4486–93.

Antal MJ, Varhegyi G. Cellulose pyrolysis kinetics: the current state of knowledge. Ind Eng Chem Res 1995; 34:703–17.

Sore S.O, Adamah Messan A., Prud'homme E., Escadeillas G., Tsobnang F. (2018), Stabilization of compressed earth blocks (CEBs) by geopolymer binder based on local materials from Burkina Faso, Construction and Building Materials 165 (2018) 333–345, https://doi.org/10.1016/j.conbuildmat.2018.01.051.

Y. Millogo, K. Traoré, R. Ouedraogo, K. Kaboré, P. Blanchart, J.H. Thomassin, Geotechnical, mechanical, chemical and mineralogical characterization of a lateritic gravels of Sapouy (Burkina Faso) used in road construction, Constr. Build. Mater. 22 (2008) 70–76, https://doi.org/10.1016 j.conbuildmat.2006.07.014.

Hussain, M.; Levacher, D.; Saouti, L.; Leblanc, N.; Zmamou, H.; Djeran-Maigre, I.; Razakamanantsoa, A. Implementation on a Preparation and Controlled Compaction Procedure for Waste-Fiber-Reinforced Raw Earth Samples. J. Compos. Sci. 2022, 6, 3. https://doi.org/10.3390/ jcs6010003.

Abbey, S.J.; Amakye, S.Y.O.; Eyo, E.U.; Booth, C.A.; Jeremiah, J.J. Wet–Dry Cycles and Microstructural Characteristics of Expansive Subgrade Treated with Sustainable Cementitious Waste Materials. Materials 2023, 16, 3124. https:// doi.org/10.3390/ma16083124.

Kathleen Dall Bello De Souza Risson Francieli S. Cofani Pinto, Gersson F.B. Sandoval, Marcos Camargo, André Campos De Moura Berenice Martins Toralles MOLDING PROCEDURE FOR PERVIOUS CONCRETE SPECIMENS BY DENSITY CONTROL, Case Studies in Construction Materials 15 (2021), https://doi.org/10.1016/j.cscm.2021.e00619.

NF P 94093 Sols, reconnaissance et essais, détermination des références de compactage d´un matériau, essai Proctor normal, essai Proctor modifié du 17 Octobre 2014.

Hu, Z.; Peng, K.; Li, L.; Ma, Q.; Xiao, H.; Li, Z.; Ai, P. Effect of Wetting-Drying Cycles on Mechanical Behaviour and Electrical Resistivity of Unsaturated Subgrade Soil. Adv. Civ. Eng. 2019, 2019, 3465327.

ASTM D559/D559M-15; Standard Test Methods for Wetting and Drying Compacted Soil-Cement Mixture1. ASTM: West Conshohocken, PA, USA, 2016.